Structure of fluoride-containing bioactive glasses

Delia S. Brauer[1,*], Natalia Karpukhina[1], Robert V. Law[2] and Robert G. Hill[1]

[1]Imperial College, Department of Materials, Exhibition Road, London SW7 2AZ, UK

[2]Imperial College, Department of Chemistry, Exhibition Road, London SW7 2AZ, UK

[*] d.brauer@imperial.ac.uk, Tel: +44-207 594 6385, Fax: +44-207 594 6757

J. Mater. Chem., 2009, 19, 5629–5636

Summary

Fluoride prevents dental cavities, stimulates bone mineralisation and decreases the melting temperature of glasses and is therefore an interesting component of bioactive glasses for use as dental or orthopaedic biomaterials. However, when designing new glass compositions, the structural role of fluoride in the glass needs to be better understood. We have characterised a glass series in the system SiO_2-P_2O_5-CaO-Na_2O with increasing concentrations of CaF_2. Network connectivity was fixed at 2.13 by adding CaF_2 while the ratio of all other components was kept constant. ^{19}F and ^{29}Si MAS NMR spectra showed that addition of CaF_2 does not cause disruption of the glass network by formation of Si-F bonds but forms mixed calcium sodium fluoride species. ^{31}P MAS NMR showed phosphate being present as orthophosphate. Hence it does not form part of the actual glass network backbone and no Si-O-P bonds are present. ^{23}Na MAS NMR showed presence of multiple sodium sites with an increase in the mean coordination number of sodium with increasing CaF_2 content. The glass transition temperature decreased with increasing amounts of CaF_2. As no Si-F bonds were formed, this can be explained by formation of hypothetical CaF^+ species. The results can be used for designing new fluoride-containing bioactive glass compositions for specific applications.

Keywords

Solid State NMR, Magic Angle Spinning NMR, Fluoride, Network Connectivity, Bioactivity

Introduction

Fluoride is well known to prevent dental decay by inhibiting enamel and dentine demineralisation, enhancement of remineralisation and inhibition of bacterial enzymes.[1,2] One key step in caries prevention is the formation of fluorapatite, which is more acid resistant than carbonated hydroxyapatite, the main component of enamel and dentine. Fluoride is also known to increase bone density and despite some dispute on dose and effectiveness in prevention of fractures, it is of interest for treatment of osteoporosis.[3,4] For these reasons addition of fluoride to bioactive glasses and ceramics is of great interest for the development of dental or orthopaedic biomaterials.[5,6] However, if we want to successfully design new bioactive glass compositions, we need to know the glass structure.

Bioactive glasses are known to form an intimate bond to bone due to formation of a hydroxycarbonate apatite (HCA) layer on their surface when in contact with body fluids due to dissolution processes.[7] Their bone bonding ability makes bioactive glasses of interest for use as bone replacement materials and coatings of metallic implants but also dentifrices[8] and in all these applications fluoride would be beneficial. The structure of silicate glasses can be described as a crosslinked inorganic polymer of oxygen and silicon. Glass properties may be explained on the basis of network connectivity (NC) which is the number of bridging oxygen atoms (BO) per network forming element.[9] Thus pure silica glass has a NC of 4 while a glass structure consisting of linear $[SiO_3]_n^{2n-}$ chains has a NC of 2. NC can be used to predict glass surface reactivity, solubility or the likelihood of undergoing glass-in-glass phase separation and bioactivity.[9,10] In general, reactivity and solubility change dramatically at a network connectivity of 2, which is the point where the glass structure changes from a crosslinked network to linear chains of decreasing molar mass. The lower the network connectivity of a glass, the lower its glass transition temperature and the greater its reactivity and solubility. Thus NC is a helpful tool when designing new bioactive glass compositions.

Solid-state nuclear magnetic resonance (NMR) is an ideal modern tool for investigation of glass structure as NMR is element specific and highly sensitive to the local chemical environment of atoms containing magnetically active nuclei. For instance, ^{19}F magic angle spinning (MAS) NMR is known to be an excellent technique for providing information on the local structure in fluoride-containing silicate glasses. ^{29}Si and ^{31}P MAS NMR are widely used to monitor next neighbours and the silicon and phosphorus environments in glasses and it can determine the Q^n structure. In addition, we take advantage of the ^{23}Na MAS NMR which is recognised as a sensitive probe of sodium environment in amorphous and crystalline materials**.**

The purpose of this study was to examine fluoride-containing bioactive glasses and the effects of fluoride incorporation on glass structure, thermal properties and temperature behaviour. We hypothesise that in these compositions, with their large number of non-bridging oxygen (NBO), fluoride does not disrupt the glass network by formation of non-bridging fluorines (NBF), but instead remains complexed to calcium. Hence CaF_2 was added by keeping the NC and the ratio of all other components constant. Glasses were characterised using X-ray powder diffraction, differential scanning calorimetry, ^{19}F, ^{29}Si, ^{31}P and ^{23}Na MAS NMR spectroscopy.

Experimental

Glass synthesis

Glasses in the system SiO_2-P_2O_5-CaO-Na_2O-CaF_2 were produced using a melt-quench route. CaF_2 was added in increasing amounts while network connectivity (NC) and the ratio of all other components were kept constant (Table 1). In addition, one sodium-free glass was synthesised. Mixtures of analytical grade SiO_2 (Prince Minerals Ltd., UK), P_2O_5, $CaCO_3$, Na_2CO_3 and CaF_2 (all Sigma-Aldrich) with addition of < 0.1 wt% $CoCO_3$ (Alfa Aesar) to reduce the spin-lattice relaxation times for ^{29}Si NMR were melted in a platinum/rhodium crucible for 1 hour at 1430°C in an electric furnace (Lenton EHF 17/3). A batch size of approximately 100 g was used. After melting, the glasses were rapidly quenched into water to prevent crystallisation.

Table 1: Synthetic glass composition in mol% and theoretical network connectivity (NC_1 calculated assuming fluorine complexes calcium, NC_2 calculated assuming fluorine forms non-bridging fluorines attached to silicon).

Glass	SiO_2	P_2O_5	CaO	Na_2O	CaF_2	NC_1	NC_2
A	49.47	1.07	23.08	26.38	-	2.13	2.13
B	47.12	1.02	21.98	25.13	4.75	2.13	1.82
C	44.88	0.97	20.94	23.93	9.28	2.13	1.49
D	42.73	0.92	19.94	22.79	13.62	2.13	1.15
E	40.68	0.88	18.98	21.69	17.76	2.13	0.78
F	36.83	0.80	17.18	19.64	25.54	2.13	-0.01
G	33.29	0.72	15.53	17.75	32.71	2.13	-0.90
H	44.88	0.97	44.87	-	9.28	2.13	1.49

Glass characterisation

All compositions were obtained in an amorphous state as confirmed by powder X-ray diffraction experiments (XRD; Phillips PW1700, 40 kV/40 mA, CuKα, data collected at room temperature; results not shown). The glass transition temperature (T_g) and crystallisation temperatures of the glasses were determined using differential scanning calorimetry (DSC). 50 mg of glass frit were

analysed in a platinum crucible using analytical grade alumina powder as reference with a heating rate of 10 K/min.

For investigation of crystal phases, milled glass powder was heat treated in analogous fashion to the DSC experiments: Samples were heated to crystallisation onset ($T_{c,ons}$) temperature at a heating rate of 10 K/min and then were allowed to cool to room temperature without holding at $T_{c,ons}$. Crystallised phases were analysed using XRD and NMR (see below).

Solid-state MAS NMR

For solid state MAS NMR experiments, the glass was ground using a Glen Creston Gy-Ro mill for 7 min. Glass structure was analysed using ^{19}F, ^{29}Si, ^{31}P and ^{23}Na MAS NMR. Experiments were performed using Bruker 200 MHz (4.7 T) and 600 MHz (14.1 T) spectrometers. ^{19}F NMR data were collected at a Larmor frequency of 188.2 MHz under spinning conditions of 12.5 kHz in a 4 mm rotor. To avoid ringing effects from the probe, the Hahn-echo pulse sequence $\pi/2–\tau–\pi$ was applied with a $\pi/2$ pulse of 2.35 μs and the echo delay τ of 76.5 μs. A recycle delay of 10 s was used, with 16 dummy scans performed before counting. A ^{19}F NMR background signal thoroughly acquired on the fluorine-free glass of this series was subtracted from the spectra of the fluorine-containing glasses. The background suppression method (DEPTH) was used for ^{19}F NMR on crystallised glasses.[11] ^{19}F chemical shift scale was referenced using the -120 ppm peak of 1 M NaF aqueous solution as a secondary reference against $CFCl_3$. ^{29}Si MAS NMR experiments were carried out at a Larmor frequency of 39.7 MHz and spinning speed of 4.5 kHz in a 4 mm rotor using the Hahn-echo pulse sequence with the $\pi/2$ pulse of 5.25 μs and 76.5 μs echo delay τ. ^{29}Si NMR was set up using a 3 min recycle delay. The -1.5 ppm peak of tetrakis(trimethylsilyl)methane was used for reference in ^{29}Si NMR. ^{19}F and ^{29}Si NMR data were processed with 200 Hz line broadening. ^{29}Si NMR experiments on crystallised samples were performed using 36.5 μs echo delay and 50 Hz exponential filter was applied to these data. ^{31}P MAS NMR spectra were acquired at 81.0 MHz in the 4 mm rotor spinning at 4.5 kHz. 64 transients of a single pulse experiment with 2.5 μs $\pi/2$ pulse and 49 s recycle delay were collected for each sample. ^{31}P chemical shift was referenced to the signal of 85% H_3PO_4. ^{23}Na NMR was performed at 158.7 MHz in 2.5 mm and 4 mm rotors and spinning speeds of about 20-25 kHz and 15 kHz, respectively. Short pulses corresponding to the magnetisation tip angle of $\pi/12$ and 0.5 s recycle delay were used for these measurements. The spectra were referenced to a 0 ppm frequency of the signal from 1 M aqueous solution of NaCl. 50 Hz line broadening was applied before Fourier transforming of the ^{31}P and ^{23}Na NMR spectra. ^{23}Na 3QMAS NMR data were obtained using a 4-pulses sequence with 20 μs zero filter. The spectra were processed with xfshear utility of Xwinnmr Bruker software and presented in a universal scale.[12]

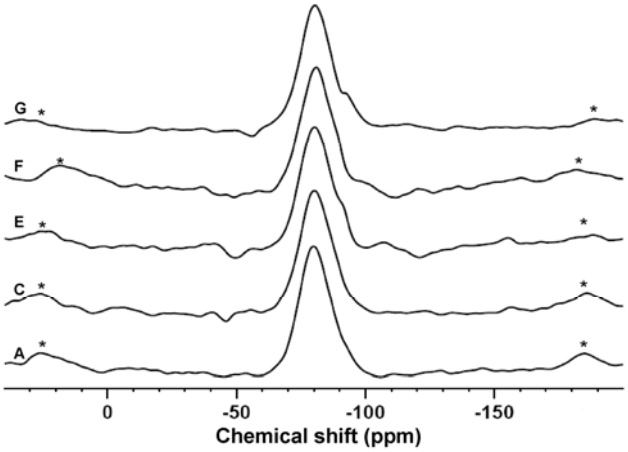

Figure 1: ^{29}Si MAS NMR spectra of glasses A, C and E to G (from bottom to top). Spinning side bands are marked by an asterisk.

Results and discussion

Structural behaviour of silicate phase

The introduction of fluoride into a bioactive glass composition did not cause formation of detectable amounts of Si-F bonds: ^{29}Si MAS NMR results (Fig. 1) show a peak at about -80 ppm which corresponds to Q^2 Si units and a shoulder at about -92 ppm indicating the presence of a small number of Q^3 Si units, which were estimated using dmfit[13] as a 10 to 14 % contribution to the signal. This is in good agreement with NC calculations assuming fluorine is binding calcium and thus reducing the availability of calcium for forming NBO (NC_1; Table 1). These calculations gave a NC of 2.13 for all glasses which corresponds to mainly Q^2 with small amounts of Q^3. If the network connectivity is calculated assuming fluorine forms NBF attached to Si (NC_2; Table 1), the values are too low to be credible. There is no change in peak (Fig. 1) position with increasing amounts of CaF_2, which suggests that formation of Si-F bonds does not occur (peaks would be expected to move to less negative chemical shift (towards 0 ppm) if there was formation of Si-F bonds in the glass which does not occur), but also that no significant amounts of fluorine were lost during melting. The absence of Si-F is in agreement with the findings by Lusvardi *et al*. who investigated the structure of fluoride-containing bioactive glasses by computational investigation.[14] Due to differences in glass design (Lusvardi *et al*. substituted CaF_2 for CaO and Na_2O, respectively) they found increased NC with increasing CaF_2 content but did not find any Si-F bonds for CaF_2 concentrations below 20 mol%, and even above 20 mol% the amount was negligible. This agrees with our NMR results presented here and with other previously reported experimental findings.[15-18]

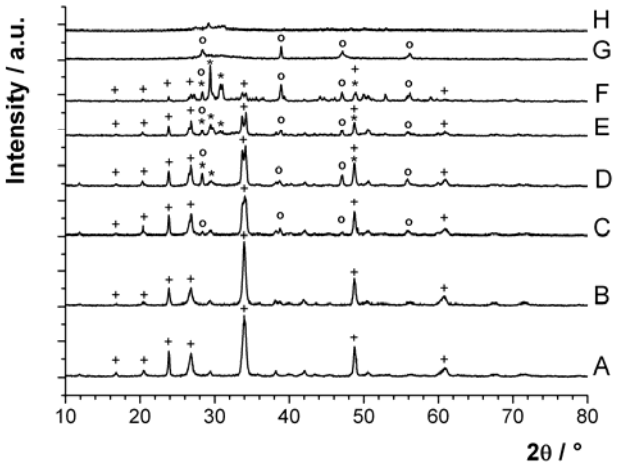

Figure 2: XRD patterns of heat-treated crystalline samples A to H (from bottom to top). Crystal phases are combeite (+), cuspidine (∗) and calcium fluoride (○).

After heat-treatment, the fluorine-free sample (A) shows combeite ($Na_2Ca_2Si_3O_9$) as the main crystal phase as determined by XRD (Fig. 2). It also shows some additional peaks of low intensity which we were not able to assign. With increasing amounts of CaF_2 in the composition, calcium fluoride (CaF_2, samples B to F) and cuspidine ($Ca_4Si_2O_7F_2$, samples C to F) appear as additional crystal phases. Sample G, which has the highest fluorine content gives only a single crystal phase which is calcium fluoride. Sodium-free sample H only crystallised to a small degree and therefore the XRD pattern shows only a few peaks, which makes interpretation problematic.

The main peak for combeite at about 34° 2θ (Fig. 2) appears as a single peak for glasses A and B and only appears as the typical split peak for higher concentrations of CaF_2. It was shown that mixed calcium sodium silicate glasses crystallise through the formation of solid solutions of several phases including combeite of different stoichiometry and a $Na_4CaSi_3O_9$ phase.[19] In sodium-rich glasses A and B we assume additional precipitation of $Na_4CaSi_3O_9$[20] which gives the principal XRD peak at about 34° 2θ overlapping with the split reflections of combeite. Absence of this phase on the XRD patterns of the compositions starting from C can be explained by the decrease in sodium content in the compositions.

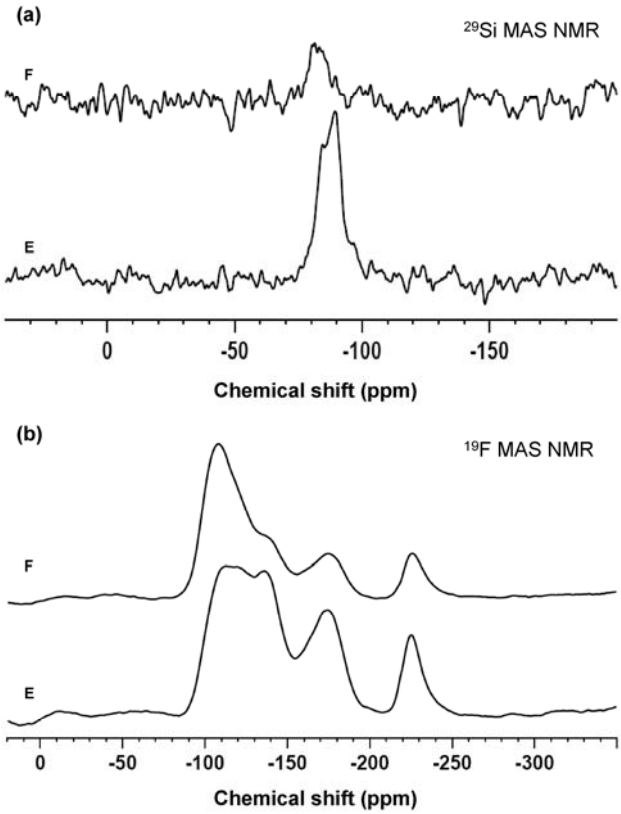

Figure 3: (a) ^{29}Si MAS NMR spectra of heat-treated crystalline samples E (bottom) and F (top) and (b) ^{19}F MAS NMR spectra of heat-treated crystalline samples E (bottom) and F (top).

^{29}Si MAS NMR spectra (Fig. 3a) for the heat-treated crystalline sample E show peaks in the range of Q^3 (-85 ppm) and Q^4 (-90 ppm). However, Q^2 in ring structures gives similar chemical shifts as Q^4[20]. As the six-membered ring combeite[21] is the main crystal phase, the peak at -90 ppm corresponds to one of the sites in the silica ring.[20,22] The peak at -85 ppm can then be explained by the remaining glass phase, which after crystallisation of combeite has a higher NC and therefore mostly a Q^3 structure. The fact that combeite is the main crystal structure in glasses A to E also suggests that in the amorphous glasses silica ring structures might also be present. This can explain the position of the Q^3 shoulder (-92 ppm) which is more negative than usually assigned to Q^3 units.

The presence of cuspidine detected by XRD is consistent with the change in ^{29}Si NMR peak position (-82 ppm) towards Q^1 structure for crystallised sample F (Fig. 3a). Cuspidine has not been obtained as a single crystalline phase in our glasses unlike in low sodium glasses of Hayashi *et al*.[23] This is primarily because of a lower NC of 1.6 for the glasses designed by Hayashi *et al*. compared to our compositions.

Structural role of fluoride and sodium ions

In the ^{19}F MAS NMR spectrum (Fig. 4) of the sodium-free glass (H) a single peak at -89 ppm corresponds to F-Ca(n) species as observed previously in calcium fluorosilicate glasses.[16,17] This

peak is at higher chemical shifts than F-Ca(4) or F-Ca(3) in crystalline species due to slightly longer Ca-F distances in amorphous glasses.[24] In glasses B to G the peak at about -220 ppm is close to position of the hexa-coordinated F-Na(6) species[25] and, thus, corresponds to complexes with sodium.

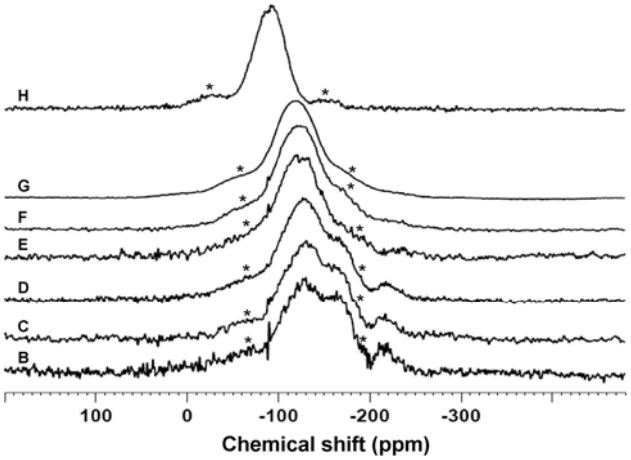

Figure 4: ^{19}F MAS NMR spectra of glasses B (bottom) to H (top). Spinning side bands are marked by an asterisk. Peak positions according to deconvolution are found in the supporting information.

The signals between -115 and -165 ppm (Fig. 4) can be assigned to mixed sodium calcium fluoride species.[26,27] Hayashi *et al*.[26] report their chemical shifts relative to hexafluorobenzene (C_6F_6), conversion to the scale relative to trichlorofluoromethane ($CFCl_3$) using a -164.9 ppm chemical shift value for C_6F_6 are found in Table 2. Their spectra show three broad peaks, which the authors assign to a) F-Ca(4), F-Ca(3)Na(1) and F-Ca(2)Na(2) species in tetrahedral coordination, b) F-Ca(1)Na(4) in pentahedral coordination and c) F-Na(6) in hexahedral coordination.

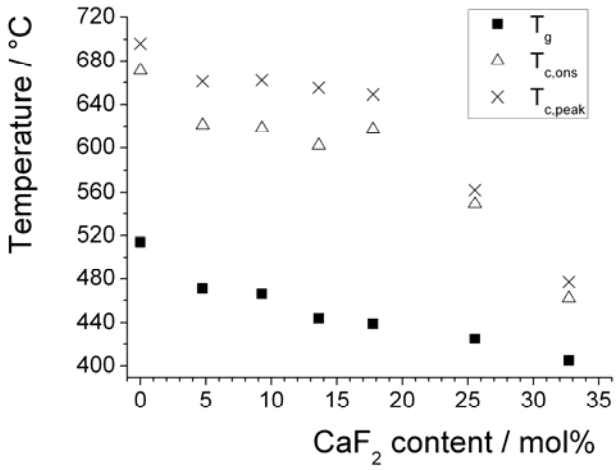

Figure 5: Glass transition temperature (T_g), crystallisation onset ($T_{c,ons}$) and crystallisation peak ($T_{c,peak}$) temperatures *vs*. CaF_2 content. The error is less than the size of the points.

For glasses B to D we clearly see three main peaks at about -130, -165 and -220 ppm (Fig. 4). The peak at -165 ppm we assign to F-Ca(2)Na(2) species whereas the observed signals at -130 ppm in

glasses B to D and -115 ppm in E to G are attributed to overlapping/unresolved signals from F-Ca(4) (at -108 ppm) and F-Ca(3)Na(1) (at -138 ppm). Presence of 5- or 6-coordinated fluorine in mixed calcium/sodium environment in this region should also be considered. Due to the high calcium concentration in glasses E to G the dominating contribution from F-Ca(4) causes the shift of the total signal towards the site of F-Ca(4).

Table 2: ^{19}F MAS NMR chemical shift references found in literature.[25,26]

Species	^{19}F Chemical Shift in ppm	
	relative to C_6H_6	relative to $CFCl_3$
F-Ca(4)	60.5	-104.4
F-Ca(3)Na(1)	58.3	-106.6
F-Ca(2)Na(2)	50.6	-114.3
(tetrahedral	38.1	-126.8
coordination)	32.0	-132.9
	26.4	-138.5
F Ca(1)Na(4)	-8.2	-173.1
(pentahedral	-9.9	-174.8
coordination)	-10.4	-175.3
	-10.9	-175.8
F-Na(6)	-56.6	-221.5
(hexahedral	-59.4	-224.3
coordination)	-62.0	-226.9
Si-F-Ca(n)	-	-123
		-129
		-135
Si-F-Na(2)	-	-152

^{19}F MAS NMR spectra of the heat treated samples (Fig. 3b) demonstrate a significant increase in structural order of the fluoride sites compared to the untreated glasses. This is consistent with the fluorine containing phases identified on XRD patterns (fluorite and cuspidine). In addition to peaks at about -175 and -225 ppm, the spectra of heat-treated crystalline samples E and F clearly illustrate that the broad peak between about -115 and -130 ppm actually consists of at least two individual peaks at about -108 and -138 ppm. The signal from cuspidine is not clearly resolved on the ^{19}F NMR spectra due to severe overlaps in the region from -100 to -110 ppm. We assign the peak at -175 ppm in the crystalline samples to a mixed sodium calcium coordination which is an intermediate to the pure sodium site F-Na(6) at -225 ppm. Hayashi *et al*.[26] assigned this to a pentahedral coordination of fluorine in F-Ca(1)Na(4), however, we do not exclude the possibility that it could be hexahedral F-Na(4)Ca(2) species.

For higher fluorine concentrations, the relative intensities of the ^{19}F NMR peaks in the region from -165 to -225 ppm in glasses and their crystalline counterparts decreases and only shoulders are visible for some of these resonances. This is caused by the fact that with increasing amounts of

CaF_2 the concentration of sodium decreases and thus fluorine preferentially complexes calcium, rather than sodium.

The ^{19}F NMR data presented above provides further evidence for the absence of NBF and Si-F-Ca(n) and Si-F-Na(n) species, the signals of which would be expected in the range between -123 and -152 ppm (Table 2).[25] This is in agreement with the findings by Hayashi *et al*. who investigated the effect of fluorine addition on the network connectivity of glasses in the system SiO_2-CaO-CaF_2 using X-ray photoelectron spectroscopy (XPS)[18]. According to their results fluorine does not affect the network connectivity or the concentration of NBO, but is coordinated with Ca^{2+}. This was further confirmed by ^{19}F NMR investigations by Watanabe *et al*.[28] In glasses with a network connectivity around 2, the presence of Si-F bonds is unlikely since there is a large concentration of NBO in the glasses and Si^{4+} has a higher affinity for O^{2-} ions than for F^- ions.[16] Thus this strongly suggests that fluorine complexes only calcium and sodium.

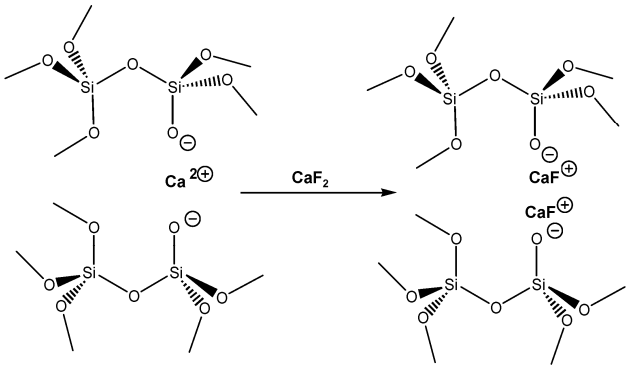

Figure 6: Illustration of the hypothetical effect of CaF_2 addition on silicate network.

Transition temperature (T_g) of the glasses decreased with increasing CaF_2 content (Fig. 5) which further indicates that fluorine was not lost in significant amounts. Crystallisation onset ($T_{c,ons}$) and peak ($T_{c,peak}$) temperatures also decreased with increasing CaF_2 content. The decrease in T_g can also be explained by the fact that fluorine is complexing calcium: in fluorine-free glass A, divalent calcium ions bind together silicate anions by electrostatic forces and the calcium ions effectively act as ionic bridges between two NBO. When CaF_2 is added (Fig. 6), hypothetical CaF^+ species are added to the silicate ions which reduces the electrostatic forces between non bridging oxygens considerable and results in a decrease in T_g.[18,29,30]

^{23}Na MAS NMR spectra of glasses A, C and E to G (Fig. 7) exhibit a single broad peak centred between -1 and -5 ppm. Despite the broadness of the peaks there do appear to be sites within the glass between 4 and 7 ppm, with a sharp feature at 4 ppm which is particularly pronounced in sample A. In glass ceramics, the ^{23}Na MAS NMR signal from NaF varies between 5 and 7 ppm depending on the crystal size.[31] Therefore, the appearance of a small shoulder at *ca*. 7 ppm can be explained by complexing of sodium with fluorine with increasing fluorine concentrations. After

crystallisation (Fig. 8), a very sharp peak appears at 7 ppm due to an increase in structural order of the fluorine environment as seen in ^{19}F MAS NMR.

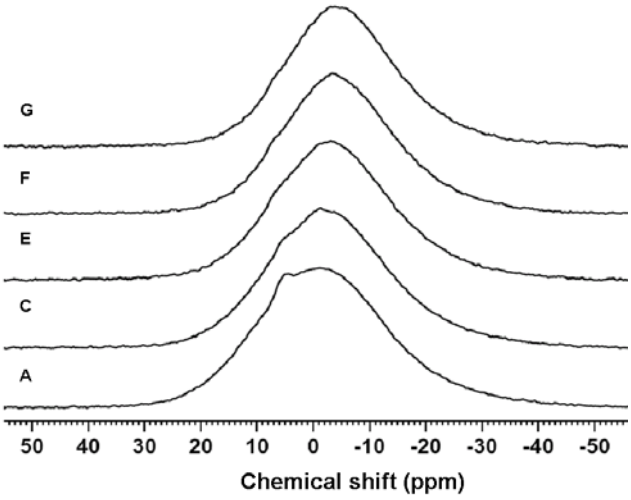

Figure 7: ^{23}Na MAS NMR spectra of glasses A, C and E to G.

Gradual replacement of combeite by the fluorine containing phases cuspidine and fluorite, which was seen in XRD results, should be expected to be associated with the evolution of the ^{23}Na NMR signal of the crystallised samples (Fig. 8) at 13 and -1 ppm along the series. Unfortunately, there are no ^{23}Na NMR reference spectra for combeite crystals of any stoichiometry. Moreover, the precipitation of a $2Na_2SiO_3$-$CaSiO_3$ or $Na_4CaSi_3O_9$ phase in sodium rich compositions of the series (as seen from the XRD data) additionally complicates interpretation of the ^{23}Na NMR spectra for the crystalline samples. The broad peak at -1 ppm for crystallised sample G (Fig. 8) is likely to be caused by the significant amount of glassy phase found by XRD (Fig. 9).

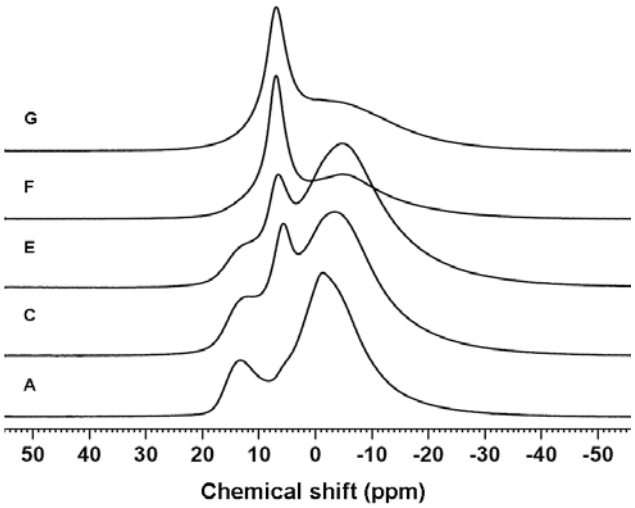

Figure 8: ^{23}Na MAS NMR spectra of crystalline samples A, C and E to G.

^{23}Na 3QMAS NMR spectra for samples A and G are given in Figs. 10 and 11 and confirm the presence of multiple sodium sites in the glasses. The distinctive shoulder in the fluorine-free glass (A) appearing on the MAS spectrum (Fig. 7) at 4 ppm has an isotropic chemical shift at *ca*. 8 ppm

overlapping to a broad featureless signal as seen in Fig. 10. This result agrees with the simulation of the ^{23}Na 3QMAS NMR experimental spectrum for Bioglass® 45S5 containing at least three different sites[32] with one of them giving a distinctively narrow resonance. The origin of this narrow signal is not clear and could also arise from the surface hydration. Comparison of these deconvolution results with an NMR study on bioactive glasses by Lockyer *et al*.[33] indicates that the broad site perhaps dominates in the low field spectra, giving a nearly -10 ppm value for MAS shift at 8.45 T. In the glass with the highest fluorine content (glass G) the signal becomes broader, but does show at least two lines one of which has the larger quadrupolar constant (site I), as shown in Fig. 11, but as in glass A no sharp features are detected. A slight shift to more negative values of the broad ^{23}Na resonance indicates an increase in the mean coordination number of sodium in glasses[34] moving from A to G, probably arising from a decrease in sodium content within the series. This is consistent with the observations by Lusvardi *et al*.[14]

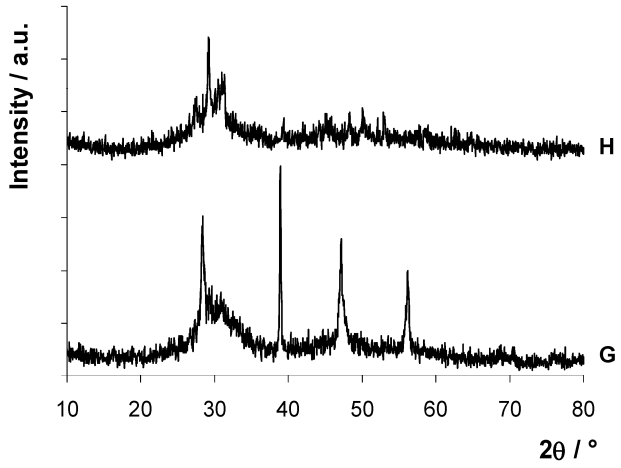

Figure 9: XRD patterns of heat-treated crystalline samples G (bottom) and H (top) showing crystalline diffraction pattern superimposed on an amorphous halo.

Structural role of phosphate

^{31}P MAS NMR spectra (Fig. 12) show a single peak corresponding to orthophosphate, Q^0, which shows that phosphate is not part of the actual glass network backbone and no Si-O-P bonds are present. These findings are in contrast to the modelling results by Lusvardi *et al*. who found that increasing amounts of fluoride ions forces phosphate groups to bond to silicon atoms by removing the modifier ions Ca and Na from the silicate glass network.[14] Orthophosphate groups are charge balanced by cations, which in our glasses are Na^+, Ca^{2+} and the hypothetical CaF^+ species. While we introduce CaF_2 into the glass, chemical shift of the orthophosphate peak moves from 9 ppm (glass A) to 6 ppm (glass G) and 3 ppm (sodium-free glass H). This agrees with the findings by Lockyer *et al*. and Elgayar *et al.* who substituted CaO for Na_2O in bioactive glass compositions and observed a shift to less positive peak positions (towards 0 ppm) with increased amounts of CaO.[10,33]

Lockyer *et al*. explained this by differences in the electronegativities of Na^+ and Ca^{2+}, which result in displacement of charge from the oxygen and hence from the P-O bond. This increases the electronic shielding of the phosphorus and produces a more negative chemical shift.

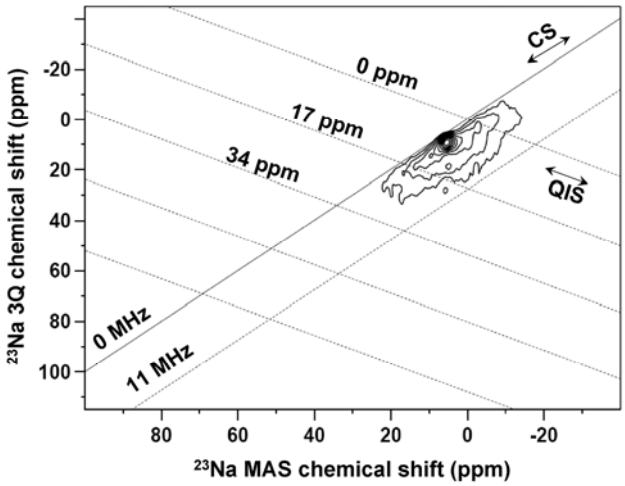

Figure 10: ^{23}Na 3QMAS NMR spectrum of glass A. The lines inside the spectrum illustrate the position of the isotropic chemical shift and quadrupolar product. The distribution of isotropic chemical shift (CS) and quadrupolar isotropic shift are indicated by arrows. 10 contours are drawn every 10% from 10 to 100% of spectral intensity.

Alternatively, the higher field of the Ca^{2+} cation drives the ^{31}P chemical shift towards more negative values compared to the effect of the lower potential of Na^+.[35] In our system, however, we have an additional species potentially contributing to the chemical shift of orthophosphate, the hypothetical CaF^+ unit. We therefore compared our ^{31}P MAS NMR results with those in the literature.[10,33,36] Fig. 13 illustrates the ^{31}P isotropic chemical shift trend graphically: It shows the ^{31}P NMR chemical shift *vs.* calcium as a fraction of total calcium and sodium (each expressed in at%) and our results show very good agreement with those found in the literature. Thus, the hypothetical CaF^+ species do not seem to contribute to the charge balancing of the orthophosphate species and the evolution of the ^{31}P chemical shift is governed by the reduction of the sodium proportion in glasses A to G. Additionally, the results in Fig. 13 reveal the disordered character of the phosphate environment, *i.e*. the cations charge balancing the orthophosphate units while CaF_2 is introduced in glass. This indicates that there is no preferential association with either sodium or calcium ions, and these will therefore be present in a ratio consistent with that of the overall glass composition.[33] This differs from the conclusions of Lusvardi et al. who suggested an ultimate preference of the phosphate units for calcium cations.[14] We would expect formation of mixed sodium calcium orthophosphates during crystallisation in our glasses, although the amount of this phase is perhaps too low for detection by XRD.

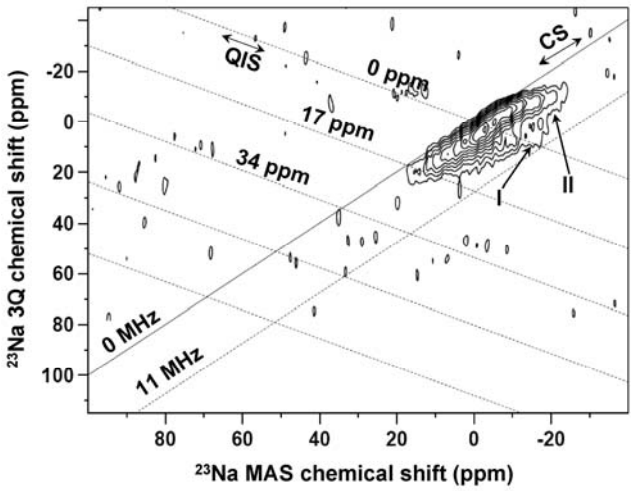

Figure 11: ^{23}Na 3QMAS NMR spectrum of glass G. The lines inside the spectrum illustrate the position of the isotropic chemical shift and quadrupolar product. The distribution of isotropic chemical shift (CS) and quadrupolar isotropic shift are indicated by arrows. 10 contours are drawn every 10% from 10 to 100% of spectral intensity. Features of at least two different sites are distinguished: site I has a larger quadrupolar constant than site II.

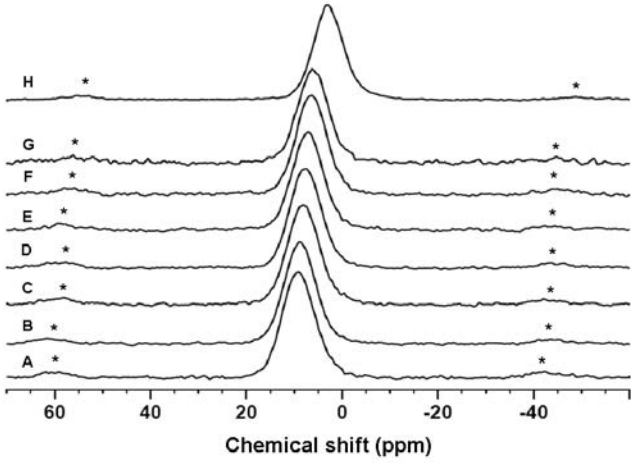

Figure 12: ^{31}P MAS NMR spectra of glasses A (bottom) to H (top). Spinning side bands are marked by an asterisk.

Impact on bioactivity

The knowledge of the structure of fluoride-containing bioactive can be applied to previous studies of bioactive glasses in the literature: Table 3 shows four compositions taken from Fuji *et al*.[37] Using the fact that fluorine complexes Ca and Na, we have calculated the theoretical and experimental NC which determines the proportions of the Q^n species present and can also be used to predict the bioactivity. There is an excellent agreement between our predicted NC and their experimental determined values (Table 3). Furthermore taking the value of a NC = 2.4 as the cut off for bioactivity,[9] the bioactivity of the glasses can be successfully predicted: The glass (F10C40S50)

with a theoretical NC of 2.4 gave an experimental NC of 2.60. *In vitro* formation of apatite in simulated body fluid is often taken as an indicator of bioactivity[38] and glass F10C40S50 showed no formation of apatite within one week while all other compositions with NC below 2.4 did.

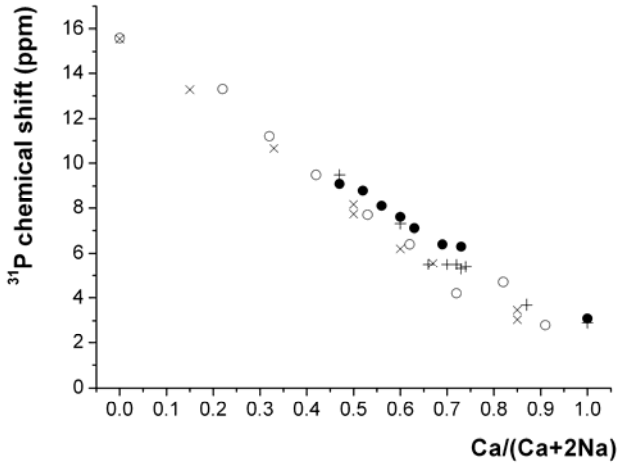

Figure 13: ^{31}P MAS NMR chemical shift *vs*. calcium content as a fraction of total calcium and sodium (all in at%): • our results, + Elgayar *et al*.[10], ○ Lockyer *et al*.[33] and × Grussaute *et al*.[36]

This shows that a) NC calculations can be used to successfully predict the bioactivity of glasses and b) knowledge of the glass structure is very important when designing new bioactive glasses.

Table 3: Synthetic glass composition in mol%, theoretical (NC calculated assuming fluorine complexes calcium) and experimental network connectivity species and experimental bioactivity (in terms of formation of an apatite layer in simulated body fluid within 3 days) of glasses by Fujii *et al*.[37]

Glass	SiO_2	CaO	NaF	theor. NC	exp. NC (NMR)	Bioactive
C50S50	50	50	0	2.0	2.11	yes
F10C40S50	50	40	10	2.4	2.60	no
F10C45S45	45	45	10	2.0	2.05	yes
F10C50S40	40	50	10	1.5	1.63	yes

Conclusions

To our knowledge, this is the first multi-nuclei characterisation of the structure of fluoride-containing bioactive glasses. Our detailed structural investigations result in a thorough understanding of the structure-property relationship in this class of bioactive glasses. We have demonstrated that in fluoride-containing bioactive glasses formation of Si-F bonds or non-bridging fluorines does not occur to a significant extent. Instead, fluorine complexes calcium and sodium and is present principally as mixed calcium sodium fluoride species. This means that if calcium fluoride is substituted for network modifiers such as CaO or Na_2O, it results in crosslinking of the network,

an increase in network connectivity and thus reduced reactivity and bioactivity of the glass. By assuming that fluorine complexes calcium and keeping the ratio of network former to network modifier constant when adding calcium fluoride, network connectivity and subsequently bioactivity are kept constant. The results of this study will be valuable in designing and producing new fluoride-containing bioactive glasses for use as reconstructive material for bone and other hard tissue, but they are also of interest for the design of other fluoride-containing silica glass systems with a high concentration of non-bridging oxygens, e.g. mould flux systems.

References

1 J. D. B. Featherstone. *Journal of the American Dental Association*, 2000, **131**, 887-899.

2 T. T. Thuy, H. Nakagaki, K. Kato, P. A. Hung, J. Inukai, S. Tsuboi, H. Nakagaki, M. N. Hirose, S. Igarashi and C. Robinson. *Arch Oral Biol*, 2008, **53**, 1017-1022.

3 P. Vestergaard, N. R. Jorgensen, P. Schwarz and L. Mosekilde. *Osteoporosis International*, 2008, **19**, 257-268.

4 J. Aaseth, M. Shimshi, J. L. Gabrilove and G. S. Birketvedt. *Journal of Trace Elements in Experimental Medicine*, 2004, **17**, 83-92.

5 W. Vogel and W. Höland. *Angewandte Chemie-International Edition in English*, 1987, **26**, 527-544.

6 Hench LL, Spilman DB, Hench JW, inventors; University of Florida U, assignee. Fluoride-modified bioactive glass (Bioglass) and its use as implant material. US patent 4775646. 1988 Oct 4.

7 L. L. Hench. *Journal of Materials Science-Materials in Medicine*, 2006, **17**, 967-978.

8 B. J. Tai, Z. Bian, H. Jiang, D. C. Greenspan, J. Zhong, A. E. Clark and M. Q. Du. *Journal of Clinical Periodontology*, 2006, **33**, 86-91.

9 R. Hill. *Journal of Materials Science Letters*, 1996, **15**, 1122-1125.

10 I. Elgayar, A. E. Aliev, A. R. Boccaccini and R. G. Hill. *Journal of Non-Crystalline Solids*, 2005, **351**, 173-183.

11 D. G. Cory and W. M. Ritchey. *Journal of Magnetic Resonance*, 1988, **80**, 128-132.

12 J. P. Amoureux and C. Fernandez. *Solid State Nuclear Magnetic Resonance*, 1998, **10**, 211-223.

13 D. Massiot, F. Fayon, M. Capron, I. King, S. Le Calve, B. Alonso, J. O. Durand, B. Bujoli, Z. H. Gan and G. Hoatson. *Magnetic Resonance in Chemistry*, 2002, **40**, 70-76.

14 G. Lusvardi, G. Malavasi, M. Cortada, L. Menabue, M. C. Menziani, A. Pedone and U. Segre. *Journal of Physical Chemistry B*, 2008, **112**, 12730-12739.

15 R. Hill, D. Wood and M. Thomas. *Journal of Materials Science*, 1999, **34**, 1767-1774.

16 R. G. Hill, N. Da Costa and R. V. Law. *Journal of Non-Crystalline Solids*, 2005, **351**, 69-74.

17 Q. Zeng and J. F. Stebbins. *American Mineralogist*, 2000, **85**, 863-867.

18 M. Hayashi, N. Nabeshima, H. Fukuyama and K. Nagata. *Isij International*, 2002, **42**, 352-358.

19 V. M. Fokin and E. D. Zanotto. *Journal of Non-Crystalline Solids*, 2007, **353**, 2459-2468.

20 J. Schneider, V. R. Mastelaro, H. Panepucci and E. D. Zanotto. *Journal of Non-Crystalline Solids*, 2000, **273**, 8-18.

21 H. Ohsato, Y. Takeuchi and I. Maki. *Acta Crystallographica Section C-Crystal Structure Communications*, 1986, **42**, 934-937.

22 M. D. O'Donnell, S. J. Watts, R. V. Law and R. G. Hill. *Journal of Non-Crystalline Solids*, 2008, **354**, 3554-3560.

23 M. Hayashi, T. Watanabe, K. Nagata and S. Hayashi. *Isij International*, 2004, **44**, 1527-1533.

24 N. Boden, P. K. Kahol, A. Mee, M. Mortimer and G. N. Peterson. *Journal of Magnetic Resonance*, 1983, **54**, 419-426.

25 T. J. Kiczenski and J. F. Stebbins. *Journal of Non-Crystalline Solids*, 2002, **306**, 160-168.

26 M. Hayashi, T. Watanabe, H. Nakada and K. Nagata. *Isij International*, 2006, **46**, 1805-1809.

27 J. F. Stebbins and Q. Zeng. *Journal of Non-Crystalline Solids*, 2000, **262**, 1-5.

28 Watanabe T, Hayashi M, Hayashi S, Fukuyama H, Nagata K. Solid-state F-19 NMR on CaO-SiO2-CaF_2 glasses. Johannesburg: The South African Institute of Mining and Metallurgy; 2004 p. 699-706.

29 T. Bååk and A. Ölander. *Acta Chemica Scandinavica*, 1955, **9**, 1350-1354.

30 P. M. Bills. *Journal of the Iron and Steel Institute*, 1963, **201**, 133-140.

31 J. W. Zwanziger, U. Werner-Zwanziger, E. D. Zanotto, E. Rotari, L. N. Glebova, L. B. Glebov and J. F. Schneider. *Journal of Applied Physics*, 2006, **99**.

32 A. Angelopoulou, V. Montouillout, D. Massiot and G. Kordas. *Journal of Non-Crystalline Solids*, 2008, **354**, 333-340.

33 M. W. G. Lockyer, D. Holland and R. Dupree. *Journal of Non-Crystalline Solids*, 1995, **188**, 207-219.

34 X. Y. Xue and J. F. Stebbins. *Physics and Chemistry of Minerals*, 1993, **20**, 297-307.

35 R. J. Kirkpatrick and R. K. Brow. *Solid State Nuclear Magnetic Resonance*, 1995, **5**, 9-21.

36 H. Grussaute, L. Montagne, G. Palavit and J. L. Bernard. *Journal of Non-Crystalline Solids*, 2000, **263**, 312-317.

37 E. Fujii, K. Kawabata, H. Yoshimatsu, S. Hayakawa, K. Tsuru and A. Osaka. *Journal of the Ceramic Society of Japan*, 2003, **111**, 762-766.

38 T. Kokubo and H. Takadama. *Biomaterials*, 2006, **27**, 2907-2915.